J Appl Electrochem (2016) 46:807–817
DOI 10.1007/s10800-016-0928-2

RESEARCH ARTICLE

Graphene-linked graphitic carbon nitride/TiO_2 nanowire arrays heterojunction for efficient solar-driven water splitting

Jingyang Su[1] · Ping Geng[2] · Xinyong Li[3] · Guohua Chen[1,2]

Received: 1 December 2015 / Accepted: 16 January 2016 / Published online: 15 February 2016

Abstract A novel structure composed of TiO_2 nanowire arrays (NWAs) was designed and synthesized by decorating with graphene-linked graphitic carbon nitride (GCN) layers. It serves as a robust photoanode for high-performance solar-driven water splitting in an alkaline solution. The GCN layers were deposited on TiO_2 NWAs by a facile electrophoretic method, producing an interconnected two-dimensional GCN nanosheets/one-dimensional TiO_2 NWAs heterostructure. Under simulated solar light illumination (light intensity 100 mW cm^{-2}), the optimal GCN/TiO_2 NWAs photoelectrode produces a photocurrent density of 1.7 mA cm^{-2} at 1.23 V versus reversible hydrogen electrode (RHE), which is around 2.6 times enhancement from that of pristine TiO_2 (0.7 mA cm^{-2} at 1.23 V vs. RHE). The photo-conversion efficiency of GCN/TiO_2 NWAs is up to 0.92 % at a low bias potential 0.50 V versus RHE, 3.6 times higher than pristine TiO_2 (0.27 % at 0.59 V vs. RHE). The improved photoelectrochemical activity is mainly because of the improved charge separation and transport within the heterojunction as well as enhanced light absorption.

✉ Guohua Chen
kechengh@ust.hk

[1] Environmental Engineering Program, School of Engineering, The Hong Kong University of Science and Technology, Clear Water Bay, Kowloon, Hong Kong, China

[2] Department of Chemical and Biomolecular Engineering, The Hong Kong University of Science and Technology, Clear Water Bay, Kowloon, Hong Kong, China

[3] Key Laboratory of Industrial Ecology and Environmental Engineering (Ministry of Education, China), School of Environmental Science and Technology, Dalian University of Technology, Dalian 116024, China

Graphical Abstract

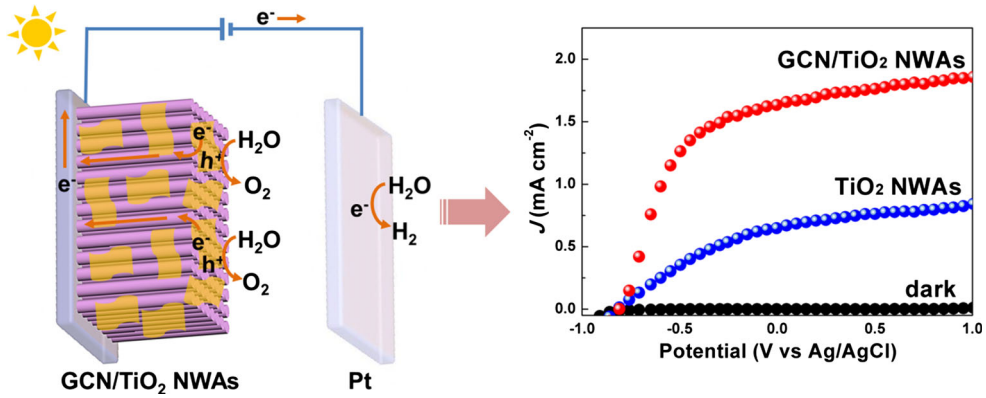

Keywords TiO_2 nanowire arrays · Graphitic carbon nitride · Photoelectrochemical · Water splitting

1 Introduction

Photoelectrochemical (PEC) water splitting using earth-abundant elements has been widely investigated as an efficient approach to convert abundant solar energy to clean hydrogen energy since 1972 [1–6]. Among various photocatalysts, TiO_2 is an ideal semiconductor material for efficient water splitting because of its high surface area [7–9], excellent stability [10, 11], efficient charge transfer [12, 13], and nice biological compatibility [14]. Vertically oriented TiO_2 nanowire arrays (NWAs) have been developed through a simple hydrothermal reaction with highly ordered morphology, good rutile crystallinity, and improved PEC performance [15, 16]. However, the solar-to-hydrogen efficiency of TiO_2 NWAs is still very low which is limited by its large band-gap energy (3.0–3.2 eV) [17, 18] and fast electron–hole recombination (usually <100 ns) [19–21]. Construction of a semiconductor heterojunction has been considered as an effective strategy to improve the PEC activity, in which the prepared heterojunction can improve charge transfer and separation between different semiconductors because of the internal electric field formed [11, 22–25]. Various semiconductors have been explored to enhance PEC activity of TiO_2 NWAs, such as CdS [26–28], CdSe [29, 30], ZnO [31], $ZnIn_2S_4$ [32], and carbon nanodots [33]. However, stability and efficiency are often compromised with these strategies, limiting the large-scale applications. Thus, there is an urgent need to develop a synergistic TiO_2-based multicomponent photoelectrode system with simultaneously improved efficiency and stability.

Graphitic carbon nitride (g-C_3N_4) is a new kind of promising metal-free semiconductor developed recently [34]. Many reports have demonstrated that it is able to produce hydrogen or oxygen from water under visible light irradiation [34–37]. However, it suffers from low electric charge transport and fast charge recombination [38, 39]. Graphene-linked g-C_3N_4 (GCN) can provide efficient charge transport and separation ability via a π–π stacking interaction between graphene and g-C_3N_4, as reported previously [40]. Herein, GCN, which was prepared by insertion of graphene into g-C_3N_4, as a sensitizer was fabricated to construct a heterojunction with TiO_2 NWAs for improved PEC capability. The prepared GCN/TiO_2 heterostructure photoelectrode is expected to possess significantly improved PEC activity for efficient water splitting under solar light illumination.

2 Experimental section

2.1 Synthesis of TiO_2 NWAs

The rutile TiO_2 NWAs were synthesized on clean fluorine-doped tin oxide (FTO) conductive glasses using the hydrothermal method as reported in the previous works [16, 41]. In a typical synthesis, 0.67 mL titanium butoxide (TBOT) was added into 40 mL 6 M HCl solution. After stirring for 15 min, the solution was poured into a Teflon-lined stainless steel autoclave until the clean FTO substrates were immersed in the solution. The autoclave was sealed and heated to 170 °C for 7 h in an oven. After the reaction, the autoclave was removed from the oven, and allowed to cool to room temperature naturally. The obtained electrode was washed sequentially with DI water and absolute ethanol before it was annealed at 500 °C for 2 h in air.

2.2 Fabrication of exfoliated GCN

The graphite oxide (GO) was produced by the modified Hummer's method [42], and the details can be found in our

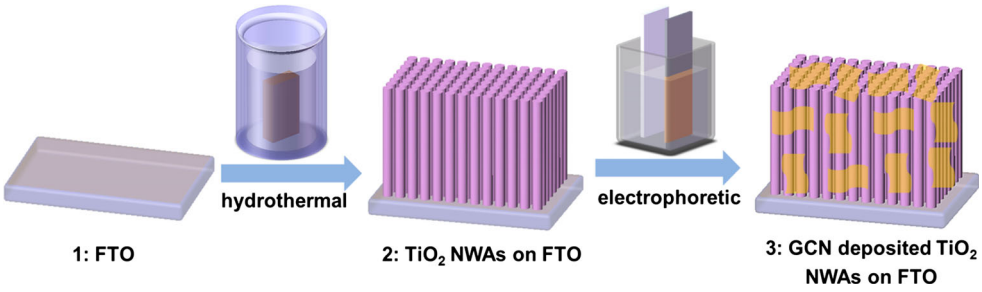

Fig. 1 Preparation process of GCN/TiO_2 NWAs heterojunction. **1** FTO glass; **2** TiO_2 NWAs on FTO through hydrothermal; **3** GCN deposited on TiO_2 NWAs by electrophoresis

previous publications [23, 43]. Then GCN bulk was prepared through a thermal polymerization process in argon atmosphere. Specifically, 10 mL exfoliated GO aqueous solution (2 mg mL^{-1}) was mixed with 2 g dicyandiamide with a ratio of 1:100, and then the mixture was put into a quartz vessel and heated to 550 °C for 4 h in argon atmosphere. The produced bulk material was hand-ground with an agate mortar. Then the prepared bulk sample was dispersed in a 2-isopropanol solution with the concentration of 0.3 mg mL^{-1} and exfoliated by ultrasonic at room temperature for 12 h. The produced mixture was separated through centrifugation at 3000 rpm for 10 min. Afterwards, the supernatant was collected carefully by pipette. The concentration of exfoliated GCN nanosheets was determined as around 0.12 mg mL^{-1} by drying the mixture.

2.3 Preparation of GCN/TiO_2 NWAs heterojunction

GCN nanosheets were deposited onto TiO_2 NWAs by an electrophoretic process according to the previous reports [23, 44]. TiO_2 NWAs electrode and stainless steel electrode were used as the cathode and anode, respectively. The applied voltage was 60 V. The amount of GCN on the TiO_2 NWAs can be changed by regulating the time of electrophoresis. After electrophoresis, the prepared sample was taken out and dried in a N_2 stream, then annealed at 350 °C for 1 h under an argon atmosphere to improve the contact between GCN and TiO_2. The schematic diagram of the whole preparation process of GCN/TiO_2 NWAs is shown in Fig. 1.

2.4 Characterization

Surface morphologies of TiO_2 NWAs and GCN/TiO_2 NWAs were examined by field emission scanning electron microscopy (FESEM, JEOL 7100F) and high-resolution transmission electron microscope (HRTEM, JEOL JEM2010F). X-ray diffraction (XRD) analysis was conducted by X-ray diffractometer (PANalytical, X'pert Pro) equipped with a Cu $K\alpha$ radiation source (wavelength of 1.54 Å). X-ray photoelectron spectroscopy (XPS) was recorded on a PHI 5600 (Physical Electronic, USA) equipped with an Al monochromatic X-ray source. C 1 s line at 284.6 eV was used as the calibration reference before each measurement.

2.5 PEC performance test

PEC measurements were conducted in a conventional three-electrode cell system. The prepared electrode was employed as the working electrode. Meanwhile, a saturated Ag/AgCl electrode and a platinum electrode served as the reference and counter electrode, respectively. Potentials versus Ag/AgCl were converted to the reversible hydrogen electrode (RHE) by the following equation $E_{RHE} = E_{Ag/AgCl} + 0.197 + 0.059$ pH. 1 M sodium hydroxide solution (pH 13.7) acted as the electrolyte. A 300 W high-pressure xenon short arc lamp (Newport) was employed as the simulated solar light source to provide a light intensity of 100 mW cm^{-2}. Prior to measurements, the electrolyte was thoroughly deaerated by purging it with nitrogen gas for 30 min.

3 Results and discussion

3.1 Morphology

Surface morphology of prepared TiO_2 and GCN/TiO_2 NWAs was investigated by FESEM. From Fig. 2a, one can see that the synthesized TiO_2 NWAs through hydrothermal method can cover the entire surface of the FTO substrate uniformly. From its cross-sectional image, the as-prepared nanowires show a highly perpendicular orientation on the FTO glass with a length around 3 μm (Fig. 2a inset). With higher magnification, the TiO_2 nanowires can be seen to show a uniform quadrilateral structure with an average side width around 100–200 nm (Fig. 2b).

The amount of deposited GCN layers can be controlled by electrophoretic time. When the electrophoretic time increased from 15 to 60 s, the amount of GCN layers increased rapidly, demonstrating that electrophoresis is an effective approach to deposit GCN layer on TiO_2 substrate. Specifically, only limited GCN nanosheets can be observed in the SEM image after 15 s electrophoretic depositing (Fig. 3a). Depositions with 30 and 45 s gave enhanced

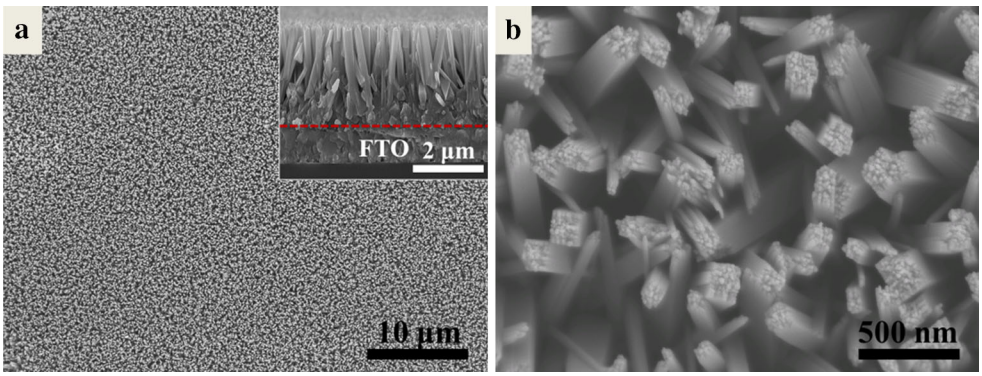

Fig. 2 Representative SEM images of prepared TiO_2 NWAs: **a** ×2500 magnification (*inset* is cross-sectional image) and **b** ×50,000 magnification

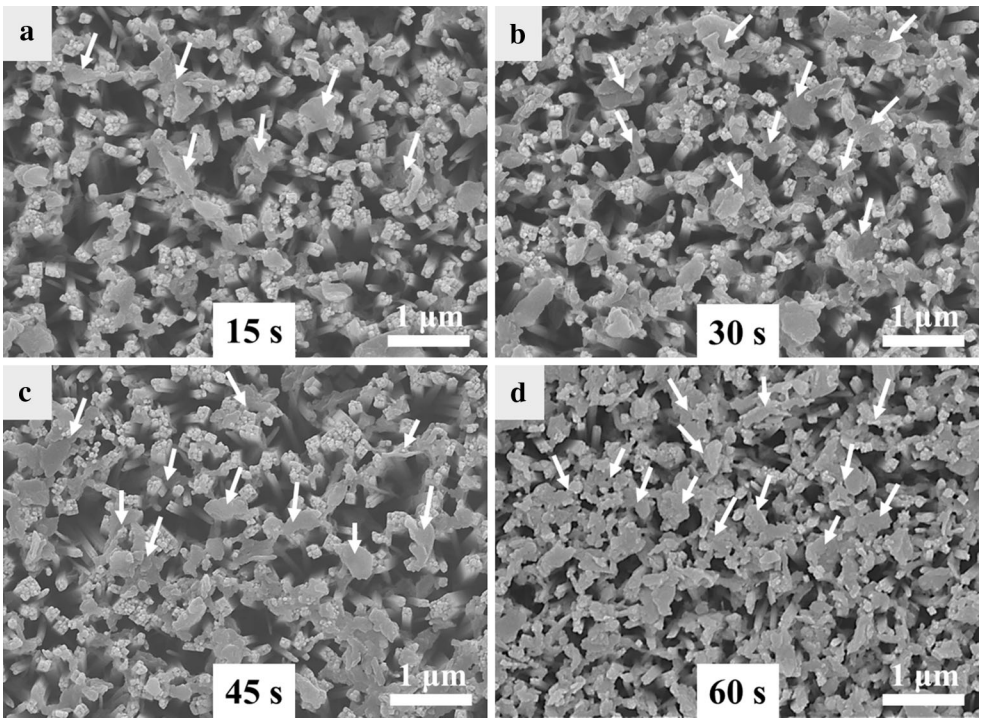

Fig. 3 Representative SEM images of GCN-modified TiO_2 NWAs with different electrophoresis time: **a** 15 s; **b** 30 s; **c** 45 s; and **d** 60 s

amounts of GCN layers with the time increase, which are compact on the surface and interspace between TiO_2 nanowires without obvious aggregation (Fig. 3b, c). It is noteworthy that the deposited GCN layers were so flexible that they can connect with TiO_2 nanowires, producing a porous and three-dimensional GCN cross-linked TiO_2 structure. This interconnected structure not only can realize dual-light absorption of TiO_2 and GCN, but also can benefit separation of photo-generated carriers and transfer to the surface of heterojunction to react with water. When electrophoretic time increased to 60 s, the TiO_2 substrate is nearly fully covered by GCN, and nanowire structure is difficult to be seen (Fig. 3d). In this case, excessive GCN layers may block efficient light absorption and photo-generated carrier transport of TiO_2, resulting in decreased PEC activity as indeed seen subsequently.

3.2 Composition

The TEM and HRTEM images of the GCN/TiO_2 NWAs detached from the FTO substrate (Fig. 4) provide more morphology and crystal structure information about the synthesized heterojunction. It can be seen clearly that the produced GCN layers connected the TiO_2 NWAs and the nanosheets possess layered structure with a thickness of several nanometers. Figure 4b shows a good crystallinity

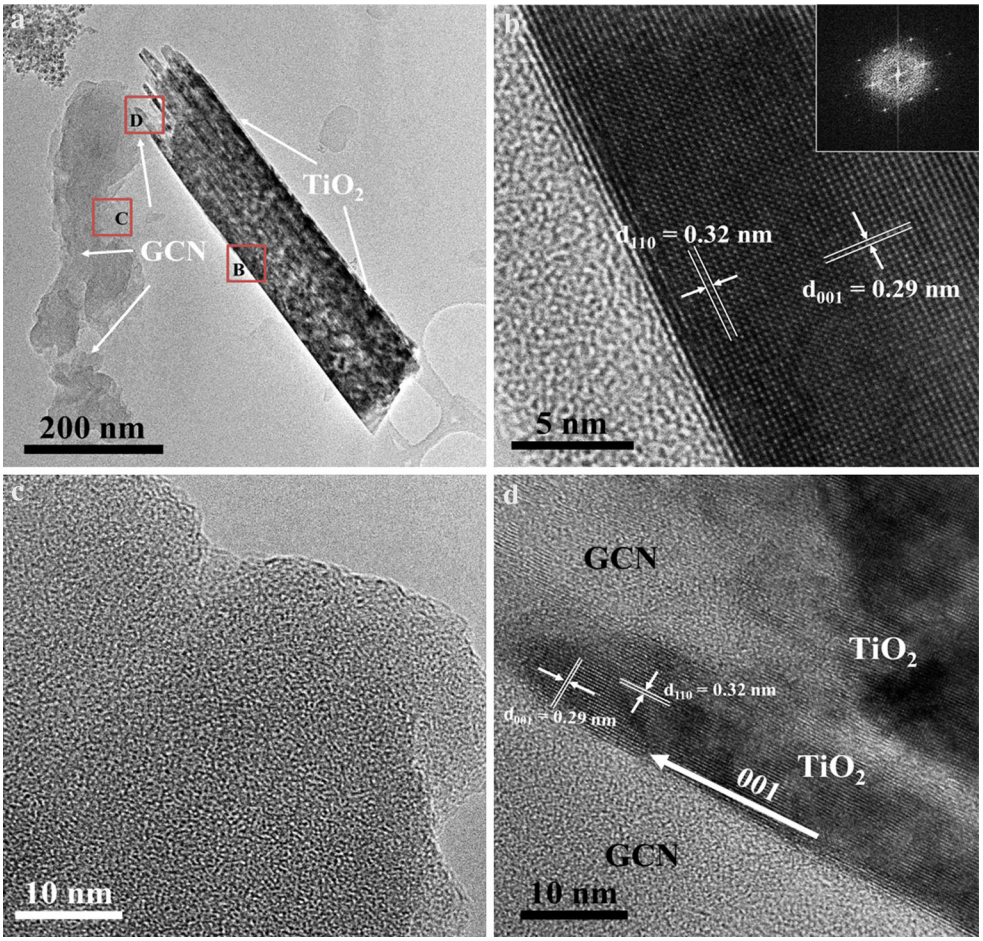

Fig. 4 **a** TEM images of GCN-modified TiO_2 NWAs at low magnification with several selected areas; **b** High magnification of marked *B*, from where a rutile phase with <001> growth direction can be identified (*inset* is the in situ SAED pattern); **c** High magnification of marked *B*, showing an amorphous crystallinity of prepared GCN, **d** The interface of heterojunction with TiO_2 nanowire and GCN (marked *D*)

of synthesized TiO_2 nanowires with interplanar spacings of 0.32 and 0.29 nm, which are consistent with the d-spacings of (110) and (001) planes of rutile TiO_2. These data further confirm the single-crystalline structure and demonstrate that the TiO_2 nanowires grow along the <100> direction. For comparison, Fig. 4c shows a representative layered structure of GCN. The thin edge of the layers indicates that the prepared GCN is only composed of few layers. This layered structure also reveals that liquid exfoliation is an effective strategy to fabricate two-dimensional nanosheets without any damage from layered bulk samples, consistent with that reported in literature [45–47]. From Fig. 4d, intimate contact was found between TiO_2 and GCN, indicating that a heterojunction can be formed between GCN layers and TiO_2 nanowires without any change in their respective morphology and crystallinity.

The crystal structure composition of pristine TiO_2 and prepared composite were further investigated using XRD and XPS. From XRD spectra (Fig. 5a), it was found that various diffraction peaks which belong to TiO_2 rutile phase were observed before and after GCN modification, revealing that prepared TiO_2 NWAs by hydrothermal reaction is pure rutile phase. Also, there are two obvious peaks centered at 13.1° and 26.5° in g-C_3N_4 spectra, which corresponds to the (110) and (200) crystal planes of g-C_3N_4, respectively. It is notable that after graphene doping (low concentration ~1 %), the two peaks of prepared GCN samples shifted slightly to 13.0° and 26.2°, respectively, revealing that the final GCN products after co-polymerization of graphene and dicyandiamide are mainly in g-C_3N_4 phase. The slight peak height decrease indicates that the interlayer distance was larger than pristine g-C_3N_4, demonstrating the successful insertion of graphene into layered g-C_3N_4, forming a novel layer-by-layer heterostructure.

XPS results (Fig. 5b) indicate the presence of Ti in the prepared samples with corresponding peaks at 459.0 and 465.0 eV for Ti 2p. As can be seen from Fig. 5c, the C 1 s peak at 284.6 eV can be ascribed to carbon and defect-

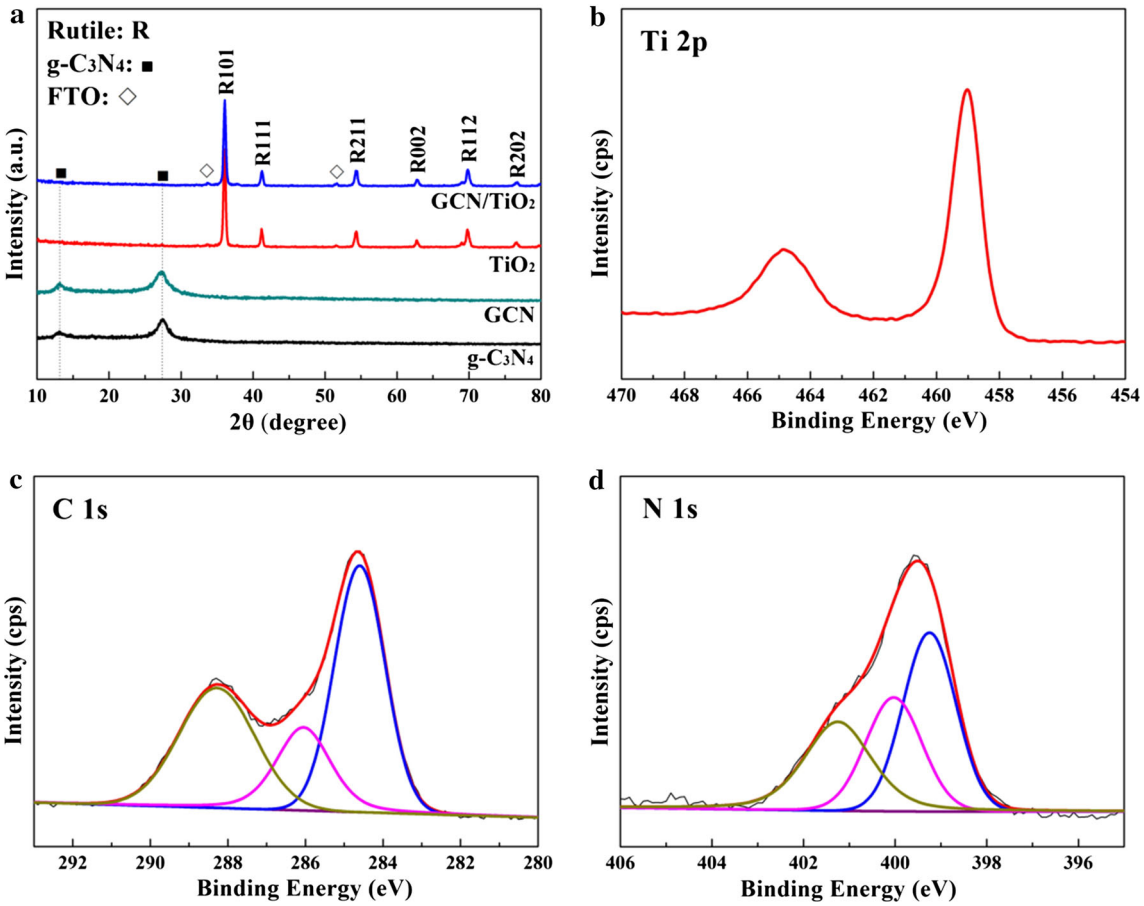

Fig. 5 **a** XRD pattern of synthesized CN, GCN, TiO_2, and GCN/TiO_2; XPS spectra of **b** Ti 2p, **c** C 1 s, and **d** N 1 s of prepared GCN/TiO_2

containing sp^2-hybridized carbon atoms present in graphitic domains. The C 1 s peak at 286.1 and 288.4 eV is assigned to the C–C bond in the turbostratic CN structure and sp^3 C–N bond of the sp^3-bonded composition, respectively [11, 47]. Furthermore, Fig. 5d shows the high-resolution N 1 s XPS spectra of the GCN/TiO_2 sample. The main N 1 s peak at the binding energy of 399.0 eV can be assigned to sp^2-hybridized nitrogen (C–N–C). The two weak peaks at about 399.9 and 401.4 eV can be attributed to tertiary nitrogen (N–$(C)_3$) and amino functional groups having a hydrogen atom (C–N–H), respectively. The presence of the N–$(C)_3$ groups confirms the polymerization of dicyandiamide [11]. The existence of amino functional groups suggests that the g-C_3N_4 product prepared by pyrolysis of dicyandiamide was incompletely condensed, which is consistent with the previous reports [48, 49].

3.3 PEC activity and stability

To investigate the PEC activity of the prepared samples, pristine TiO_2 and prepared GCN/TiO_2 NWAs with different deposition time were used as photoanodes for PEC test in a standard three-electrode PEC cell. Obviously, a maximum photocurrent density of 1.7 mA cm^{-2} is obtained at 1.23 V versus RHE for the GCN/TiO_2 NWAs sample with the deposition time of GCN 30 s, while only photocurrent density of 0.70 mA cm^{-2} for pristine TiO_2 is observed at the same condition (Fig. 6a). This result indicates that the separation rate of photo-generated holes and electrons increased for TiO_2 NWAs after GCN modification due to the formation of a heterostructure between GCN and TiO_2. However, when the deposition time of GCN further increased to 60 s, obvious decrease in photocurrent is observed ($\sim$1.15 mA cm^{-2}). This result indicates that the deposition amount of GCN is an important affecting factor for the PEC performance of resulted heterojunction. Excessive GCN nanosheets will block light absorption of TiO_2 NWAs beneath GCN, and hinder the electron transport ability of TiO_2 NWAs, resulting in an inefficient charge transfer and separation, as reported by many researches [11, 50].

Furthermore, photo-conversion efficiency (applied bias photon-to-current efficiency), which is used to evaluate the conversion efficiency from solar energy to chemical energy, was calculated using the following equation [3]:

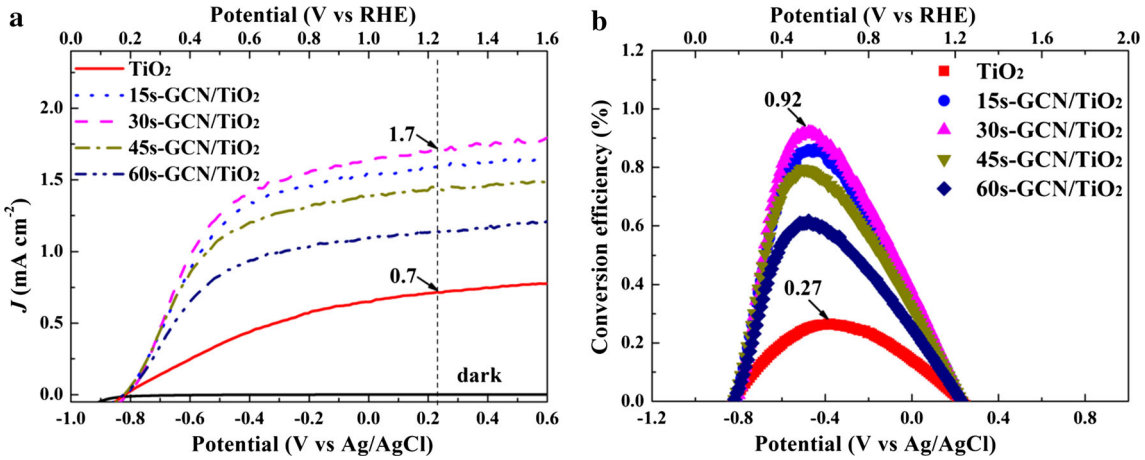

Fig. 6 **a** Linear sweep voltammetry curves of prepared TiO_2 and GCN/TiO_2 with different deposition time (0; 15; 30; 45; and 60 s) and **b** corresponding photo-conversion efficiency as a function of applied potentials

$$\eta(\%) = I\,(E^0_{\text{rev}} - V)\,/\,J_{\text{light}},$$

where η is the photo-conversion efficiency, I is the photocurrent density (mA cm^{-2}), J_{light} is the incident light irradiance (mW cm^{-2}), E^0_{rev} is the standard reversible potential which is 1.23 V versus RHE, and V is the applied bias potential versus RHE.

Figure 6b presents the plots of the photo-conversion efficiency versus applied bias potentials. The optimal photo-conversion efficiency of GCN/TiO_2 NWAs can be up to 0.92 % at a relatively low potential of 0.55 V versus RHE for GCN/TiO_2 NWAs, while pristine TiO_2 NWAs can only achieve photo-conversion efficiency of 0.27 % at 0.60 V versus RHE. The optimal photo-conversion efficiency of GCN/TiO_2 NWAs is nearly 340 % enhancement compared with pristine TiO_2 NWAs, demonstrating its significant PEC performance after GCN nanosheet modification.

To further investigate the role of GCN nanosheets in the fabricated heterostructure, the *J*–V and *J*–*t* curves were obtained for GCN bulk- and GCN sheet-modified TiO_2 NWAs in a photoelectrochemical cell under simulated solar light illumination, respectively. Clearly, both GCN bulk- and nanosheet-deposited TiO_2 NWAs display enhanced PEC performance than pristine TiO_2 due to the formation of heterojunction between GCN and TiO_2. Especially, GCN nanosheet-modified TiO_2 sample shows the highest photocurrent among all the three samples both in *J*–*V* and *J*–*t* tests. At 1.23 V versus RHE, the photocurrent density of GCN bulk/TiO_2 NWAs achieves 1.15 mA cm^{-2}, while GCN sheets/TiO_2 NWAs reaches up to 1.7 mA cm^{-2} at the same conditions, 48 % higher than that of GCN bulk/TiO_2. It is possible that GCN bulk cannot disperse onto TiO_2 uniformly, and the deposited thick-layered structure will block efficient light absorption of TiO_2 NWAs.

To further prove the hypothesis of GCN nanosheets blocking the light absorption, SEM images of both GCN bulk- and nanosheet-modified TiO_2 NWAs prepared at the same condition were taken as shown in Fig. 8. Before liquid exfoliation (Fig. 8a), the prepared GCN after polymerization shows an irregular bulk structure with the size around several micrometers. After 12 h ultrasonic liquid exfoliation, one can see clearly the uniform nanosheet structure, Fig. 8b. Furthermore, the size of the prepared nanosheets decreases to only several hundred nanometers, making it more suitable to combine with one-dimensional TiO_2 nanowire structure. As a result, GCN sheet-modified TiO_2 displays a uniform structure (Fig. 8d), where GCN nanosheets were dispersed on the surface and interspace of TiO_2 nanowires uniformly, forming an interconnected two-dimensional GCN nanosheets/one-dimensional TiO_2 nanowire heterostructure, facilitating high-performance light absorption as well as charge carrier transport within the formed heterojunction. For comparison, GCN bulk can only disperse onto TiO_2 surface due to its overlarge size (Fig. 8c). In this case, light absorption of TiO_2 would be insufficient, leading to an inefficient PEC activity of GCN bulk/TiO_2 (as shown in Fig. 7).

Furthermore, the electron recombination kinetics of GCN/TiO_2 and TiO_2 photoelectrodes were investigated by monitoring the open-circuit voltage (V_{oc}) decay as a function of time upon turning off the illumination. Under open-circuit conditions, electrons accumulate within the nanostructured semiconductor materials. Once the illumination is stopped, the accumulated electrons will be consumed by various redox reactions in the electrolyte. The electron density in the photoelectrodes decays sharply due to charge recombination, with the V_{oc} decay rate directly determined by the recombination rate. Figure 9a plots the V_{oc} decay as a function of time measured based on the

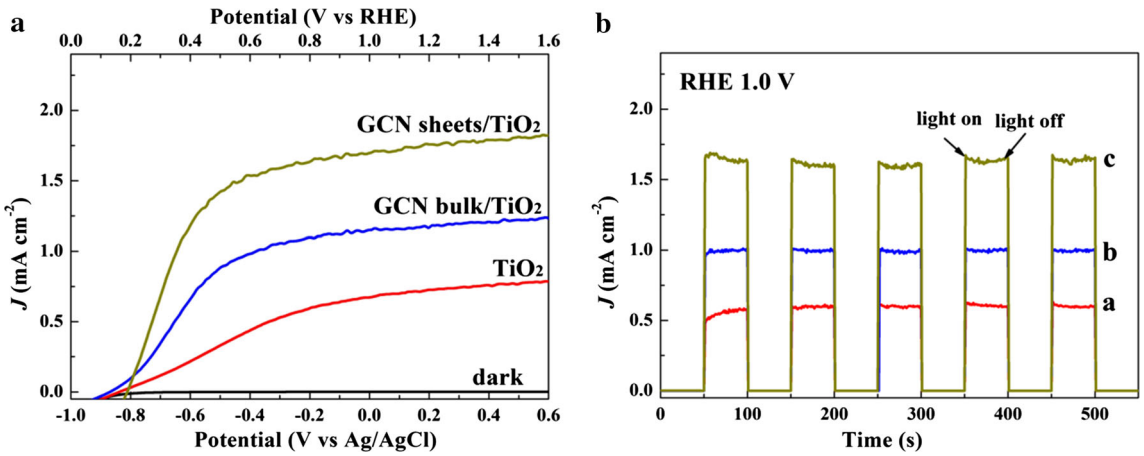

Fig. 7 Comparison of **a** photo-response of exfoliated GCN layers and prepared GCN bulk-deposited TiO_2 NWAs and **b** corresponding time-dependent photocurrent density collected at a potential of 1.0 V vs RHE (*a* TiO_2; *b* GCN bulk/TiO_2; *c* GCN sheets/TiO_2)

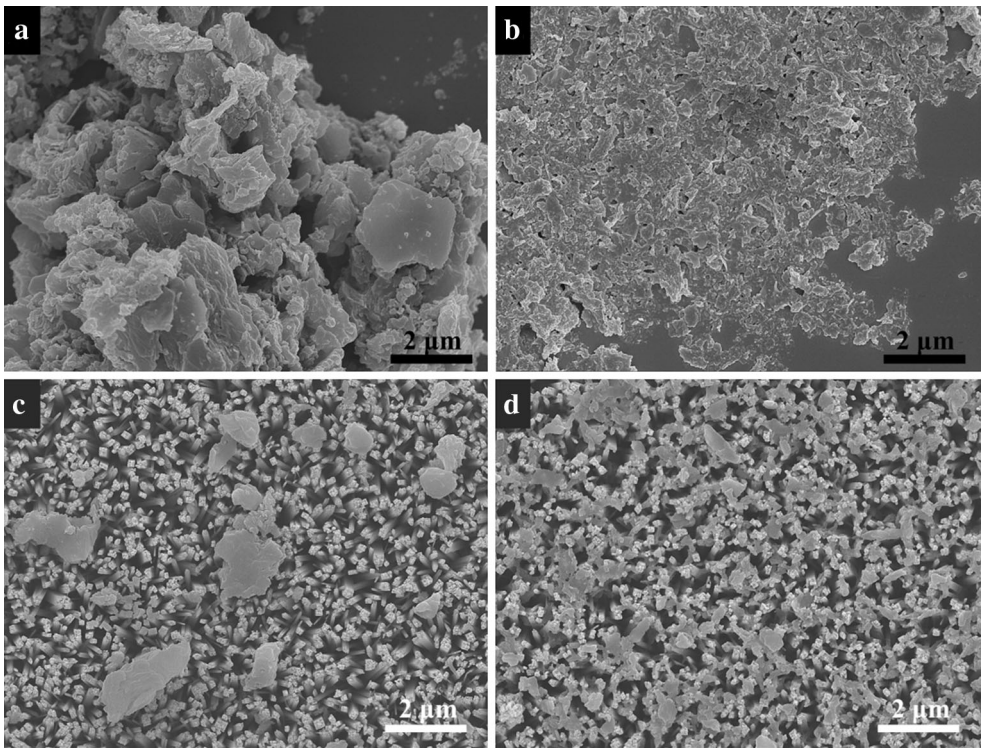

Fig. 8 Representative SEM images of **a** prepared bulk GCN; **b** exfoliated GCN layers; **c** bulk GCN-modified TiO_2 NWAs and **d** exfoliated GCN layer-modified TiO_2 NWAs (electrophoretic time is 30 s)

pristine and GCN-modified TiO_2 NWAs photoanodes. Obviously, GCN/TiO_2 NWAs electrode shows a significantly slower V_{oc} decay rate than that of pristine TiO_2 NWAs, indicating slow recombination kinetics in the prepared GCN/TiO_2 photoelectrode. The lifetime of photogenerated electrons (τ_n) can be calculated by the following equation:

$$\tau_{n=} - (k_B T/e)(dV_{oc}/dt)^{-1},$$

where k_B is Boltzmann's constant, T is the absolute temperature, and e is the elementary charge. The calculated τ_n is plotted in Fig. 9b as a function of V_{oc} for the two types of electrodes. It is observed that τ_n of the GCN/TiO_2 NWAs displays much longer time than pristine TiO_2 NWAs. The extended τ_n observed in GCN/TiO_2 NWAs compared to that observed in TiO_2 NWAs can be attributed to the surface defects formed in the GCN/TiO_2 heterostructure after

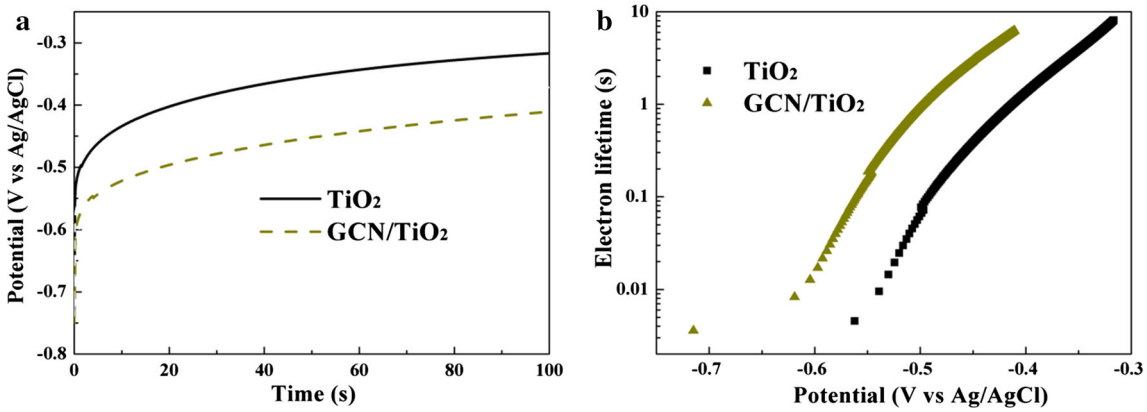

Fig. 9 **a** Open-circuit voltage decay of the GCN/TiO_2 NWAs and TiO_2 NWAs and **b** the corresponding electron lifetimes as a function of open-circuit voltage

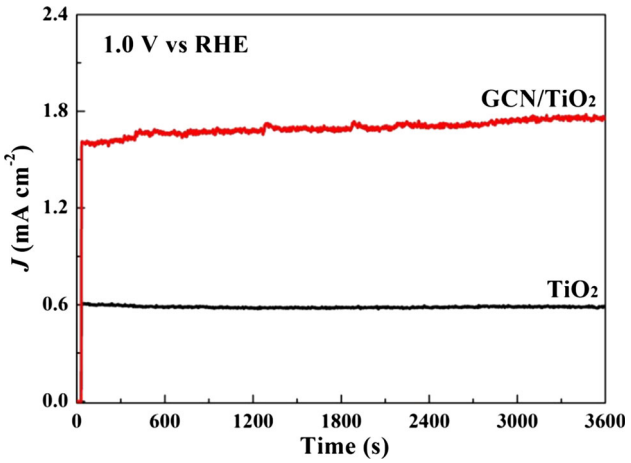

Fig. 10 Long-term stability test of exfoliated GCN/TiO_2 (1.0 V vs. RHE) under simulated solar irradiation

GCN nanosheet deposition, which can act as adsorption sites and promote the charge transport remarkably.

Moreover, the PEC stability of the GCN/TiO_2 NWAs was evaluated in a three-electrode configuration by obtaining a *J–t* curve under simulated solar light irradiation. A photocurrent density of 1.7 mA cm^{-2}, which is obtained by applying 1.0 V versus RHE on GCN/TiO_2 NWAs, was maintained for 1 h without showing any sign of decay, revealing its long-term stability (Fig. 10). Compared with the results from literature, it is notable that the stable photocurrent density of as-prepared GCN/TiO_2 NWAs collected at 1.0 V versus RHE is one of the best values reported among all the metal-free material-modified TiO_2 photoelectrodes to date (Table 1) [33, 51–53]. This excellent result can be attributed to the advantages of unique interconnected three-dimensional GCN/TiO_2 structure feature with dual-light absorption and remarkable promotion of charge transport within heterojunction interfaces.

3.4 Mechanism of charge separation and transfer

Based on aforementioned findings, the possible charge separation and transfer mechanism can be proposed for prepared GCN/TiO_2 heterojunction (Fig. 11). Under solar light illumination, GCN can be effectively excited to produce electrons and holes from conduction band (CB) and valance band (VB), respectively. Because the CB position of the GCN is more negative than that of the TiO_2, an internal local electric field is therefore generated [52, 54]. This makes the electrons generated by GCN quickly transfer to the CB of TiO_2 NWAs, going along aligned TiO_2 nanowires to the FTO substrate then further transported to the Pt counter electrode through external circuit, where the transferred electrons are consumed to reduce water for hydrogen evolution [11, 55]. On the other hand, the holes generated in the VB of the TiO_2 NWAs can transfer to the VB of GCN easily, realizing an efficient charge separation and transfer. Then the

Table 1 Comparison of the photocurrent density at 1.0 V versus RHE of this work with estimated values from literature under 100 mW cm^{-2} light intensity from Xenon lamp

Photoelectrode	Photocurrent density, mA cm^{-2}	Reference
GCN/TiO_2 nanowires	1.70	Present study
C_3N_4/TiO_2 nanotubes	1.70	[51]
C_3N_4/TiO_2 nanowires	0.90	[52]
N–C dot/TiO_2 nanowires	1.45	[33]
C dot/TiO_2 nanotubes	1.20	[53]

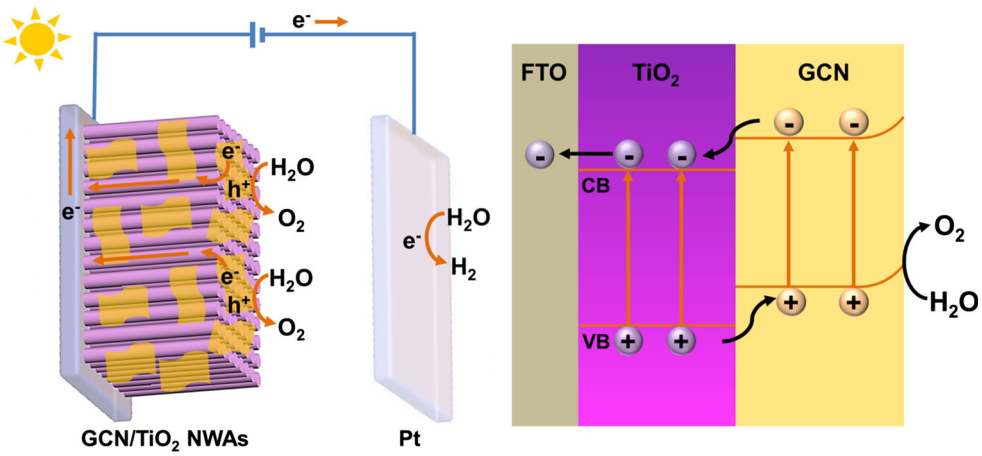

Fig. 11 Mechanism of charge transfer and separation in the prepared GCN/TiO_2 photoelectrode under solar light irradiation

produced holes of GCN and TiO_2 can oxidize water effectively [11, 56]. The efficient charge separation increases the lifetime of the charge carriers and enhances the efficiency of the interfacial charge transfer to substrates, leading to much enhanced PEC performance of the prepared GCN/TiO_2 NWAs. More importantly, the unique interconnected three-dimensional structure with multiple light absorption and large semiconductor/electrolyte interfaces is favorable for significantly improved PEC activity. This result offers a rational design and preparation strategy for TiO_2-based nanostructured photoelectrodes with improved PEC performance.

4 Conclusions

A rational GCN/TiO_2 NWA heterojunction has been fabricated as an efficient photoanode for PEC water oxidation. Under simulated solar light illumination, the photocurrent of synthesized GCN/TiO_2 NWAs can be up to 1.7 mA cm^{-2} at 1.23 V versus RHE, which is one of the best performance for all the TiO_2-based metal-free material-modified architecture. The photo-conversion efficiency of GCN/TiO_2 NWAs achieves up to 0.92 % at a low potential (0.50 V vs. RHE), 340 % enhancement from that of pristine TiO_2 (0.27 % at 0.59 V vs. RHE). Furthermore, the prepared heterojunction exhibits excellent stability, nearly 100 % retention after 1 h PEC test. The enhanced light harvest ability, improved charge transfer and separation, and unique cross-linked microstructure are responsible for the improvement of photo-conversion efficiency. This study has provided a facile and efficient strategy for fabrication and optimization of photoelectrode architecture using metal-free materials.

Acknowledgments The authors would like to thank the financial support from Hong Kong Research Grant Council under the Grant number HKUST 622813 and N_HKUST646/10.

Compliance with ethical standards

Conflict of interest The authors declare that they have no conflict of interest.

References

1. Fujishima A, Honda K (1972) Nature 238:37–38
2. Graetzel M (2001) Nature 414:338–344
3. Walter MG, Warren EL, Mckone JR, Boettcher SW, Mi Q, Santori EA, Lewis NS (2010) Chem Rev 110:6446–6473
4. Joya KS, Joya YF, Ocakoglu K, Van De Krol R (2013) Angew Chem Int Ed 52:10426–10437
5. Prévot MS, Sivula K (2013) J Phys Chem C 117:17879–17893
6. Su J, Yu H, Quan X, Chen S, Wang H (2013) Appl Catal B 138:427–433
7. Chen X, Mao SS (2007) Chem Rev 107:2891–2959
8. Thompson TL, Yates JT (2006) Chem Rev 106:4428–4453
9. Geng P, Su J, Miles C, Comninellis C, Chen G (2015) Electrochim Acta 153:316–324
10. Ma Y, Wang X, Jia Y, Chen X, Han H, Li C (2014) Chem Rev 114:9987–10043
11. Su J, Geng P, Li X, Zhao Q, Quan X, Chen G (2015) Nanoscale 7:16282–16289
12. Lee K, Mazare A, Schmuki P (2014) Chem Rev 114:9385–9454
13. Kapilashrami M, Zhang Y, Liu YS, Hagfeldt A, Guo J (2014) Chem Rev 114:9662–9707
14. Koktysh DS, Liang X, Yun BG, Pastoriza-Santos I, Matts RL, Giersig M, Serra-Rodríguez C, Liz-Marzán LM, Kotov NA (2002) Adv Funct Mater 12:255–265
15. Feng X, Shankar K, Varghese OK, Paulose M, Latempa TJ, Grimes CA (2008) Nano Lett 8:3781–3786
16. Liu B, Aydil ES (2009) J Am Chem Soc 131:3985–3990
17. Cho IS, Chen Z, Forman AJ, Kim DR, Rao PM, Jaramillo TF, Zheng X (2011) Nano Lett 11:4978–4984
18. Hoang S, Guo S, Hahn NT, Bard AJ, Mullins CB (2012) Nano Lett 12:26–32
19. Pu YC, Wang G, Chang KD, Ling Y, Lin YK, Fitzmorris BC, Liu CM, Lu X, Tong Y, Zhang JZ, Hsu YJ, Li Y (2013) Nano Lett 13:3817–3823
20. Ozawa K, Emori M, Yamamoto S, Yukawa R, Yamamoto S, Hobara R, Fujikawa K, Sakama H, Matsuda I (2014) J Phys Chem Lett 5:1953–1957
21. Yamada Y, Kanemitsu Y (2012) Appl Phys Lett 101:133907

22. Yu H, Quan X, Chen S, Zhao H (2007) J Phys Chem C 111:12987–12991
23. Yu H, Chen S, Fan X, Quan X, Zhao H, Li X, Zhang Y (2010) Angew Chem Int Ed 49:5106–5109
24. Qu Y, Duan X (2013) Chem Soc Rev 42:2568–2580
25. Mayer MT, Lin Y, Yuan G, Wang D (2013) Acc Chem Res 46:1558–1566
26. Su F, Lu J, Tian Y, Ma X, Gong J (2013) Phys Chem Chem Phys 15:12026–12032
27. Li J, Cushing SK, Zheng P, Senty T, Meng F, Bristow AD, Manivannan A, Wu N (2014) J Am Chem Soc 136:8438–8449
28. Wang H, Bai Y, Zhang H, Zhang Z, Li J, Guo L (2010) J Phys Chem C 114:16451–16455
29. Bang JH, Kamat PV (2010) Adv Funct Mater 20:1970–1976
30. Luo J, Ma L, He T, Ng CF, Wang S, Sun H, Fan HJ (2012) J Phys Chem C 116:11956–11963
31. Kayaci F, Vempati S, Ozgit-Akgun C, Donmez I, Biyikli N, Uyar T (2014) Nanoscale 6:5735–5745
32. Liu Q, Lu H, Shi Z, Wu F, Guo J, Deng K, Li L (2014) ACS Appl Mater Interfaces 6:17200–17207
33. Tang J, Zhang Y, Kong B, Wang Y, Da P, Li J, Elzatahry AA, Zhao D, Gong X, Zheng G (2014) Nano Lett 14:2702–2708
34. Wang X, Maeda K, Thomas A, Takanabe K, Xin G, Carlsson JM, Domen K, Antonietti M (2009) Nat Mater 8:76–80
35. Sun J, Zhang J, Zhang M, Antonietti M, Fu X, Wang X (2012) Nat Commun 3:1139
36. Zhang J, Chen X, Takanabe K, Maeda K, Domen K, Epping JD, Fu X, Antonietti M, Wang X (2010) Angew Chem Int Ed 49:441–444
37. Schwinghammer K, Mesch MB, Duppel V, Ziegler C, Senker J, Lotsch BV (2014) J Am Chem Soc 136:1730–1733
38. Zhang Y, Mori T, Ye J, Antonietti M (2010) J Am Chem Soc 132:6294–6295
39. Zhang G, Zhang M, Ye X, Qiu X, Lin S, Wang X (2014) Adv Mater 26:805–809
40. Zhang Y, Mori T, Niu L, Ye J (2011) Energy Environ Sci 4:4517–4521
41. Cho IS, Lee CH, Feng Y, Logar M, Rao PM, Cai L, Kim DR, Sinclair R, Zheng X (2013) Nat Commun 4:1723
42. Hummers WS Jr, Offeman RE (1958) J Am Chem Soc 80:1339
43. Xu H, Deng Y, Shi Z, Qian Y, Meng Y, Chen G (2013) J Mater Chem A 1:15142–15149
44. Su J, Yu H, Chen S, Quan X, Zhao Q (2012) Sep Purif Technol 96:154–160
45. Yang S, Gong Y, Zhang J, Zhan L, Ma L, Fang Z, Vajtai R, Wang X, Ajayan PM (2013) Adv Mater 25:2452–2456
46. Zhao H, Yu H, Quan X, Chen S, Zhang Y, Zhao H, Wang H (2014) Appl Catal B 152–153:46–50
47. Xu J, Zhang L, Shi R, Zhu Y (2013) J Mater Chem A 1:14766–14772
48. Martha S, Nashim A, Parida KM (2013) J Mater Chem A 1:7816–7824
49. Xiang Q, Yu J, Jaroniec M (2011) J Phys Chem C 115:7355–7363
50. Zhou X, Jin B, Li L, Peng F, Wang H, Yu H, Fang Y (2012) J Mater Chem 22:17900–17905
51. Yang M, Liu J, Zhang X, Qiao S, Huang H, Liu Y, Kang Z (2015) Phys Chem Chem Phys 17:17887–17893
52. Li Y, Wang R, Li H, Wei X, Feng J, Liu K, Dang Y, Zhou A (2015) J Phys Chem C 119:20283–20292
53. Zhang X, Wang F, Huang H, Li H, Han X, Liu Y, Kang Z (2013) Nanoscale 5:2274–2278
54. Zhao S, Chen S, Yu H, Quan X (2012) Sep Purif Technol 99:50–54
55. Wang J, Zhang W-D (2012) Electrochim Acta 71:10–16
56. Su J, Zhu L, Chen G (2016) Appl Catal B 186:127–135